

Trinity University

Digital Commons @ Trinity

Physics and Astronomy Faculty Research

Physics and Astronomy Department

2006

Energetics of Magnetic Storms Driven by Corotating Interaction Regions: A Study of Geoeffectiveness

Niescja E. Turner


Trinity University, nturner1@trinity.edu

E J. Mitchell

D J. Knipp

B A. Emery

Follow this and additional works at: https://digitalcommons.trinity.edu/physics_faculty

 Part of the [Astrophysics and Astronomy Commons](#)

Repository Citation

Turner, N.E., Mitchell, E.J., Knipp, D.J., & Emery, B.A. (2006). Energetics of magnetic storms driven by corotating interaction regions: A study of geoeffectiveness. In B. Tsurutani, R. McPherron, G. Lu, J.H.A. Sobral, & N. Gopalswamy (Eds.), *Recurrent magnetic storms: Corotating solar wind streams, vol. 167* (pp. 113-124). Washington, DC: American Geophysical Union.

This Contribution to Book is brought to you for free and open access by the Physics and Astronomy Department at Digital Commons @ Trinity. It has been accepted for inclusion in Physics and Astronomy Faculty Research by an authorized administrator of Digital Commons @ Trinity. For more information, please contact jcostanz@trinity.edu.

Energetics of Magnetic Storms Driven by Corotating Interaction Regions: A Study of Geoeffectiveness

Nieszcja E. Turner and Elizabeth J. Mitchell

Florida Institute of Technology, Melbourne, Florida

Delores J. Knipp

United States Air Force Academy, Colorado Springs, Colorado

Barbara A. Emery

High Altitude Observatory, National Center for Atmospheric Research, Boulder, Colorado

We investigate the energetics of magnetic storms associated with corotating interaction regions (CIRs). We analyze 24 storms driven by CIRs and compare to 18 driven by ejecta-related events to determine how they differ in overall properties and in particular in their distribution of energy. To compare these different types of events, we look at events with comparable input parameters such as the epsilon parameter and note the properties of the resulting storms. We estimate the energy output by looking at the ring current energy along with ionospheric Joule heating derived from the PC and *Dst* indices. We also include the energy of auroral precipitation, estimated from NOAA/TIROS and DMSP observations. In general, ejecta-driven storms produce more intense events, as parameterized by *Dst**, but they are usually not as long lasting, and in most cases deposit less energy. This is observed even for events that have similar input quantities, such as epsilon. This may be related to the high speed of the solar wind, in that an increased magnetosonic Mach number may influence the reconnection rate and therefore the coupling. Additionally, we find the efficiency of the coupling varies greatly from CIR-driven to ejecta-driven storms, with the CIR-driven storms coupling substantially more efficiently, particularly in the recovery phase. The efficiency of coupling (output energy divided by input energy) for CIR-driven storms in recovery phase was double that of ejecta-driven storms.

1. INTRODUCTION

1.1. Geoeffectiveness

Geoeffectiveness refers to the efficiency of energy coupling from the solar wind into the magnetosphere. It can be

estimated by looking at the solar wind input and the corresponding magnetospheric output for a particular time period. The question becomes, then, how does one quantify the solar wind input and the magnetospheric output? Solar wind input has been parameterized in several key ways over the years, usually in the form of a Poynting flux, and this remains the most widespread estimate. Magnetospheric output, however, is less clear-cut. Some use widely known magnetospheric activity indices such as *Dst* or *Kp* to estimate the response to solar wind drivers. Other researchers may be more interested in the radiation belt response, for example, and have different

approaches to quantifying that response. Since the radiation belts are less significant energetically than other sinks, they are not included in this study. For the purposes of this paper, magnetospheric response will be regarded as the total amount of energy (or, in some cases, the instantaneous power) being deposited into the primary magnetospheric energy sinks. These sinks include the ring current, ionospheric Joule heating, and auroral precipitation. As will become clear, this definition of magnetospheric response will often produce different results than other definitions, especially when it comes to defining the types of solar wind drivers that are most geoeffective.

1.2. Magnetospheric Energy Input

Precise measurements of the total amount of energy entering the magnetosphere from the solar wind are simply not possible. Over the years, however, estimates have been made. The epsilon parameter is one such estimate. Epsilon is defined (in SI units) as:

$$\varepsilon = (4\pi/\mu_0) vB^2 \sin^4(\theta/2) l_0^2$$

where v is the solar wind speed, B is the magnitude of the IMF, l_0 is a characteristic length scale representing the coupling area available for solar wind-magnetosphere interactions, usually approximated as $7 R_E$, [Perreault and Akasofu, 1978], μ_0 is the permeability of free space, and θ is defined as $\tan^{-1}(|B_Y|/B_Z)$. Epsilon is a measure of the Poynting flux in the solar wind over the magnetospheric collecting area. It uses a “leaky” filter of $\sin^4(\theta/2)$, which means that, while energy coupling is greatly enhanced for southward B_Z , there is still some coupling for northward B_Z as well. The form of epsilon is based on empirical studies of the estimated energy dissipation in the magnetosphere. Thus, while the form of epsilon is shown to replicate the pattern of energy dissipation, its scaling should be considered somewhat arbitrary, as it is based on estimates of energy output rather than quantitative knowledge of energy input. Additionally, the l_0^2 term in this equation does not vary, although the magnetopause area is known to vary with solar wind conditions [see, e.g., Monreal-MacMahon and Gonzalez, 1997].

While epsilon is the most commonly used parameterization of solar wind energy input, there are others. One effort to revisit the issue of energy input into the magnetosphere was conducted by Bargatze *et al.* [1985]. They derived a more complex coupling equation which ultimately also used the same $\sin^4(\theta/2)$ term and was similar in form to the epsilon parameter.

Other researchers parameterize solar wind energy input with vB_S , where v is the solar wind velocity and B_S is the southward component of the IMF [e.g., O’Brien and

McPherron, 2000], or would include the solar wind kinetic energy flux [e.g., Lu *et al.*, 1998]. It is likely that the actual coupling involves some combination of these, and certain parameters may become more or less dominant under different conditions. Since the kinetic energy flux is large in comparison with the epsilon-derived energy input, it would not require a very strong coupling in this regard to have a pronounced effect on the magnetosphere.

2. PREVIOUS WORK

Many researchers have investigated the flow of energy in the magnetosphere [e.g., Turner *et al.*, 2000b; Baker *et al.*, 2001; Weiss *et al.*, 1992; Vichare *et al.*, 2005]. Lu *et al.* [1998] investigated energy budgets in the magnetic storm interval that occurred in January of 1997. They used Assimilative Mapping of Ionospheric Electrodynamics (AMIE) calculations to determine the energy lost to ionospheric processes, and used the standard *Dst* index to estimate the ring current injection rate. Overall, in the January 10 and 11, 1997 case, Lu *et al.*, estimated that the magnetosphere-ionosphere system dissipated an average of about 4.0×10^{11} W. Of this, 1.9×10^{11} W (or 48%) went into Joule heating, 1.2×10^{11} W (or 30%) went into ring current injection, and 0.9×10^{11} W (or 22%) went into auroral precipitation. They did not estimate the energy lost to plasmoids streaming down the magnetotail. Knipp *et al.* [1998] analyzed the November 1993 storm, which was a hybrid event where a high-speed stream followed a CME. They found that high-speed streams could be enormously geoeffective, and for this extreme event the ionospheric heating was $\sim 190 \times 10^{15}$ J, with 30% of that generated within 24 hours of storm onset.

Gonzalez *et al.* [1989] specifically analyzed energy coupling during intense ($Dst < -100$ nT) storm events and tested the responses of several coupling functions to investigate the *Dst* response. They found that solar wind ram pressure played a role in ring current energization and that during the strong events they studied, there seemed to be a decoupling of auroral response from inner magnetospheric response for the solar wind-magnetosphere coupling functions they analyzed.

Six storms were analyzed by Turner *et al.* [2000b] to determine their energy input and deposition rates. Their calculation incorporated AMIE data to determine the ionospheric loss and a pressure- and tail-corrected form of *Dst* to track the ring current energy, and they also included a term for plasmoid ejection loss. In all cases, epsilon was shown to correlate with the energy output, and in 5 of the 6 events epsilon was estimated to be larger than the output energy. The results of this analysis showed a clear dominance of ionospheric energy deposition over other processes. In fact, Joule heating alone typically accounted for around half or more of the total energy output. The ring current contribution was less than in

previous estimates, largely due to a reevaluation of the ring current strength compared to Dst^* [Turner *et al.*, 2001, 2000a], and also due to the AMIE analysis suggesting a larger ionospheric loss. This analysis shows the ring current energy to be approximately 10%-15% of the total energy output.

The polar cap (PC) index can be used as a proxy indicator describing the amount of energy deposited into the ionosphere in the form of Joule heating and auroral precipitation. Chun *et al.* [1999], based on comparisons with AMIE data assimilation results, have shown a quadratic relationship between the PC index and the hemispheric integrated Joule heating rate, and recent work shows a linear relationship between PC and electron precipitation. More recent work by Knipp *et al.* [2004] has shown a better fit to the data if both PC and Dst are used as inputs.

The study by Turner *et al.* [2000b] of the global energy budget of the magnetosphere analyzed several storms over a fairly small time frame (about 2 years), so it was limited to a small portion of the solar cycle. It is known that solar wind driving conditions vary over the solar cycle, with corotating interaction regions (CIRs) being more common during solar minimum, and coronal mass ejections (CMEs) being more common toward solar maximum. Many researchers have observed differences in the dynamics of storms during times of different types of solar wind driving conditions, such as the existence of High-Intensity Long-Duration Continuous Auroral Activity (HILDCAA) events in the recovery phase of CIR-driven events [e.g., Tsurutani *et al.*, 2004, 2006 (this volume)]. On average, CIRs have less steady B_z and higher bulk speed than CMEs, and the resulting storms differ in some fundamental properties. Some researchers have studied the ability of different types of solar wind structures to produce storms [see, e.g., Zhang *et al.*, 2004]. Echer and Gonzalez [2004] found that compound interplanetary structures were more geoeffective than isolated structures. In another study, Huttunen *et al.* [2002] looked at storms from 1996 to 1999. They found that almost all the intense ($Dst < -100$ nT) storms were associated with CMEs, but for the moderate storms, streams more often generated high K_p storms, while ejecta-related events more often drove stronger Dst changes. This could suggest that the relative impacts on the ring current and the ionosphere could vary by type of solar wind driver. Gonzalez *et al.* [1999] found that complex interplanetary structures, including in rare circumstances the influence of subsequent CMEs, could drive particularly intense geomagnetic storms.

3. METHODOLOGY

A list of events sorted by solar wind drivers (Ian Richardson, private communication) was analyzed. These data were classified by time intervals of CMEs and CIRs during

1995-1998. Ionospheric Joule heating power was calculated according to the relations derived by Knipp *et al.* [2004]. The relations for the Joule heating in GW for the northern hemisphere are:

$$\begin{aligned} JH_{\text{summer}} &= 29.27 |PC| + 8.18 PC^2 - 0.04 |Dst| + 0.0126 Dst^2 \\ JH_{\text{equinox}} &= 29.14 |PC| + 2.54 PC^2 + 0.21 |Dst| + 0.0023 Dst^2 \\ JH_{\text{winter}} &= 13.36 |PC| + 5.08 PC^2 + 0.47 |Dst| + 0.0011 Dst^2, \end{aligned}$$

where summer is defined as 21 April – 20 August, winter is 21 October – 20 February, and equinox is 21 February – 20 April and 21 August – 20 October. For equinox times, northern hemisphere values were doubled to obtain a global value. For summer and winter dates, a Joule heating estimate for summer was added to a winter estimate to account for the hemispheric seasonal differences.

Global auroral precipitation values were computed from NOAA/TIROS and DMSP satellite measurements of high-latitude precipitating energy flux carried by ions and electrons with energies between 300 eV and 20 keV (NOAA/TIROS) or carried by electrons with energies between 460 eV and 30 keV (DMSP). The energy flux observations made during a single pass over the polar regions are used to estimate the total precipitating power input to a single hemisphere at that time. The power index was devised by Dave Evans for NOAA/TIROS and adapted for DMSP by Frederick Rich and William Denig [Emery *et al.*, 2005, 2006]. Global values were calculated by adding a southern hemisphere estimate to a northern hemisphere estimate.

All solar wind data used in this study were offset to allow propagation time from the satellite to the magnetopause.

The Dst index was pressure corrected to Dst^* using the Burton *et al.* [1975] equation, $Dst^* = Dst - b P^{1/2} + c$, where P is the solar wind dynamic pressure and the constants b and c are $b = 7.26$ and $c = 11.0$ as derived by O'Brien and McPherron [2000].

After pressure correction, the ring current energy was estimated using Dst^* . As many researchers have pointed out, [e.g., Campbell, 1996], the Dst index measures the effects of many key current systems and cannot single out the ring current. Magnetotail currents are among the primary current systems that can perturb the Dst index [see Turner *et al.*, 2000a; Ohtani *et al.*, 2001; Feldstein *et al.*, 2005], as well as induced ground currents. Dst^* was corrected to account for these using the relation described in Turner *et al.* [2001]. This calculation is made by halving the (pressure-corrected) Dst^* to remove the influence of induced ground currents and tail currents and then applying the standard Dessler-Parker-Sckopke [Dessler and Parker, 1959; Sckopke, 1966] relation. The Dessler-Parker-Sckopke (DPS) relationship between global magnetic field perturbation and particle energy is as

follows: $\Delta B = -(\mu_0/2\pi) W_{\text{particles}}/(B_0 R_E^3)$, where ΔB is approximated by the corrected Dst , $W_{\text{particles}}$ is the particle energy, μ_0 is the permeability of free space, B_0 is the surface dipole strength at the equator, and R_E is the radius of the Earth.

So, to calculate the ring current energy from Dst , the Dst index was first pressure corrected, then halved, and then plugged into the DPS relation to solve for the particle energy. The ring current injection rate was then calculated using the relationship derived by Akasofu [1981], $Q = -4 \times 10^{13} (\partial Dst/\partial t + Dst/\tau)$ in SI units, with the ring current decay time set to $\tau = 6$ hours. The epsilon parameter was used to estimate energy input.

Storm intervals were identified where Dst^* was less than -50 nT and a storm recovery phase was observed with at least 80% Dst^* recovery. From these criteria, 24 CIR-driven storms and 18 ejecta-driven storms were identified and analyzed. For a complete list of events in this study, see Tables 1 and 2.

Two example events are shown in Figure 1. A CIR-driven event from April 16-21, 1997 is shown to scale alongside a CME-driven event from April 21-23, 1997. These events are representative of the population of storms in this study with the CIR-driven event lasting approximately 2.75 times longer

Table 1. List of all CIR-driven events in the study

Start Date	Hour	End Date	Hour	Minimum Dst^*
29-Jan-95	9	5-Feb-95	5	-74.22
11-Feb-95	6	16-Feb-95	22	-52.13
7-Apr-95	1	12-Apr-95	13	-152.53
22-Apr-95	13	26-Apr-95	5	-54.56
16-May-95	4	21-May-95	12	-89.81
24-Jul-95	4	26-Jul-95	0	-55.06
2-Oct-95	5	11-Oct-95	1	-96.71
20-Oct-95	0	26-Oct-95	6	-66.28
30-Oct-95	11	4-Nov-95	22	-58.68
24-Dec-95	8	25-Dec-95	23	-66.72
10-Mar-96	11	14-Mar-96	14	-60.01
19-Mar-96	7	24-Mar-96	11	-69.72
17-Oct-96	9	26-Oct-96	17	-105.40
27-Feb-97	0	4-Mar-97	15	-92.18
16-Apr-97	18	21-Apr-97	6	-77.31
1-May-97	17	5-May-97	1	-66.29
10-Mar-98	11	14-Mar-98	12	-116.65
20-Mar-98	10	23-Mar-98	7	-87.77
24-Apr-98	1	28-Apr-98	12	-73.19
6-Jun-98	16	9-Jun-98	7	-50.37
16-Jul-98	3	18-Jul-98	5	-58.69
30-Sep-98	15	2-Oct-98	12	-57.69
2-Oct-98	14	5-Oct-98	5	-55.26
7-Oct-98	0	11-Oct-98	12	-67.41

Table 2. List of all ejecta-driven events in the study

Start Date	Hour	End Date	Hour	Minimum Dst^*
6-Feb-95	11	9-Feb-95	9	-79.23
4-Mar-95	12	7-Mar-95	4	-91.89
22-Aug-95	17	23-Aug-95	17	-60.67
18-Oct-95	13	19-Oct-95	19	-122.96
10-Jan-97	5	10-Jan-97	23	-76.16
10-Apr-97	22	11-Apr-97	15	-87.15
21-Apr-97	13	23-Apr-97	4	-106.66
15-May-97	6	18-May-97	11	-115.93
26-May-97	16	29-May-97	0	-72.48
5-Nov-97	8	9-Nov-97	8	-114.98
10-Dec-97	11	13-Dec-97	1	-60.14
6-Jan-98	16	8-Jan-98	6	-76.80
29-Jan-98	22	31-Jan-98	17	-55.16
17-Feb-98	14	20-Feb-98	10	-106.35
26-Jun-98	0	26-Jun-98	13	-100.91
6-Aug-98	3	9-Aug-98	1	-148.97
20-Aug-98	8	21-Aug-98	8	-66.47
8-Nov-98	21	11-Nov-98	9	-142.11

than the CME-driven storm and containing similar integrated epsilon values. Table 3 contains the energy, minimum Dst^* , and event duration values for these events.

Superposed epoch analyses were conducted for Dst^* , B_Z , solar wind number density, solar wind speed, magnetosonic Mach number, epsilon, ring current injection rate, Joule heating power, and auroral precipitation power. Data were separated into main phase and recovery phase as defined by the minimum Dst^* point in each event. Integrated values of the parameters were calculated for each event.

4. OBSERVATIONS

Figure 2 shows IMF B_Z for CIR and ejecta-driven storms. The CIR storms (Panel A) show rapidly varying B_Z which hovers near zero throughout the events, and continues to oscillate rapidly around $B_Z = 0$ well into the storm recovery. The ejecta storms (Panel B) show a slowly changing B_Z that gradually moves from southward to northward orientation and then largely stays northward. Panel C shows a superposition of B_Z for CIR and ejecta-related events. It is clear from the superposition that for the events in this study, when B_Z in ejecta-related drivers goes northward it stays there, allowing recovery, while CIR-driven events show a B_Z hovering near zero.

Figure 3 shows the superposed solar wind inputs of the entire set of events. Panel A shows the solar wind speed: note the much faster flows during CIR events. The second panel has the epsilon parameter, used as an indicator of input energy. For the storms in this set, the ejecta-related events

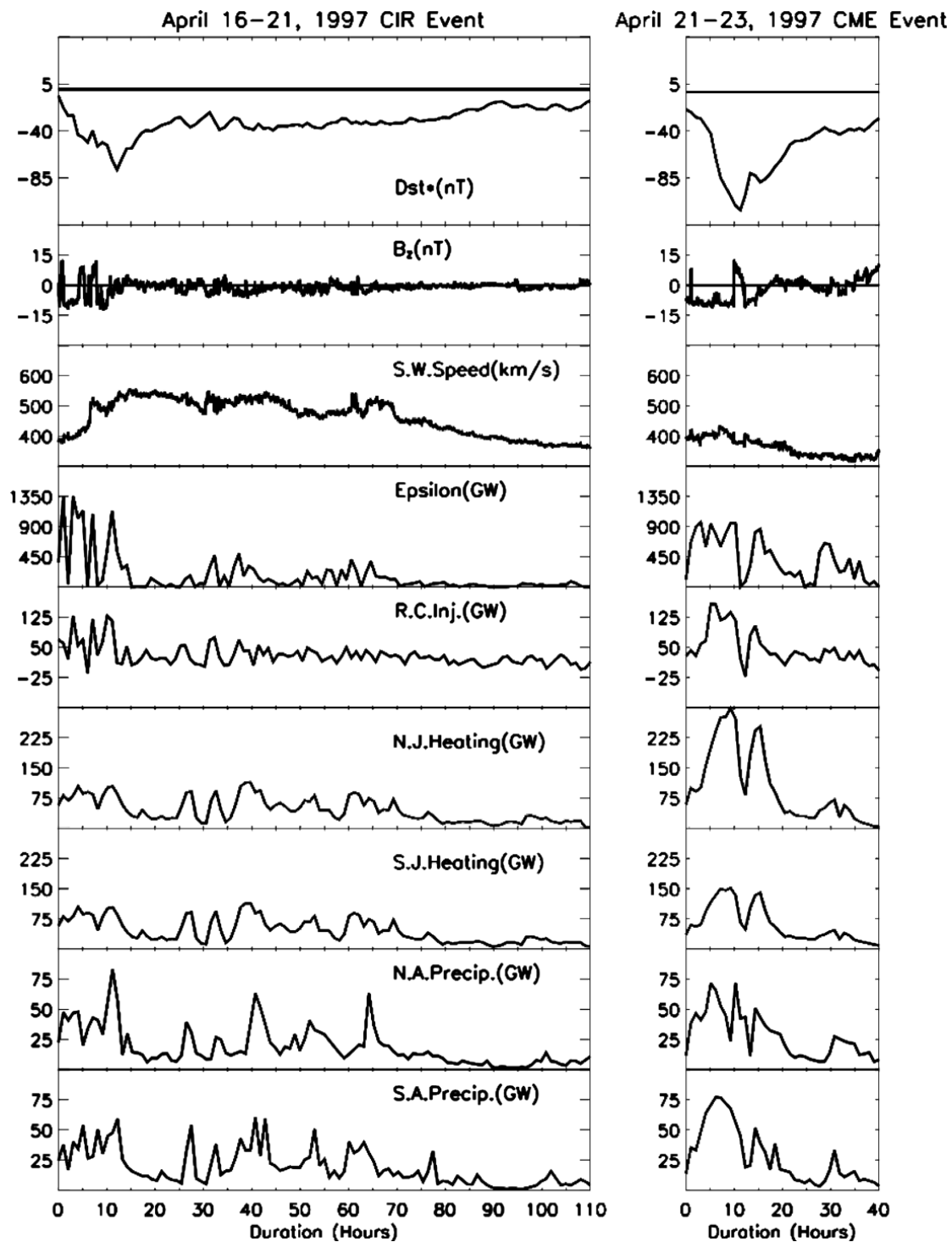


Figure 1. Two example events: a CIR-driven event on April 16-21, 1997 and a CME-driven event on April 21-23, 1997.

Table 3. Table of energies, minimum Dst^* , and event durations for example events in Figure 1

Type of Event	Date	Duration (Hours)	Min Dst^* (nT)	Input (10^{15} J)	Ring Current (10^{15} J)	Joule Heating (10^{15} J)	Auroral Precipitation (10^{15} J)
CIR Event	Apr 16-21, 1997	109	-77.31	62.60	11.24	35.19	14.73
Ejecta Event	Apr 21-23, 1997	40	-106.66	60.02	6.75	23.42	8.04

show a higher epsilon during the main and early recovery phases. Epsilon peaks about 3 hours before the Dst^* minimum, and is nearly double for ejecta what is it for CIRs. The magnetosonic Mach number is plotted in Panel C, and again indicates the much faster flows common to CIR events. Panels D and E show the Joule heating and ring current injection rates, respectively, with both showing only a moderate advantage for ejecta-driven events. Panel F shows the superposed Dst^* , which shows the clear advantage of ejecta-driven events in producing large Dst^* excursions.

Figure 4 shows the total energy output for all studied events. While the input energies are similar for the CIR and

ejecta events, the output quantities are larger and outside the error bars for every measured quantity. The duration of the CIR storms, it should also be noted, is substantially larger than for ejecta storms, which could play a role in allowing greater energy deposition and may be a result of continuing driving of the system well into the recovery.

In Figure 5 the averaged energy per hour for all storms in the dataset is shown. The input power for ejecta-driven storms is about double that for CIR-driven storms, and the Dst^* is somewhat higher for them as well. The output power for ring current, auroral precipitation, and Joule heating are larger for the ejecta events, but not nearly with the same

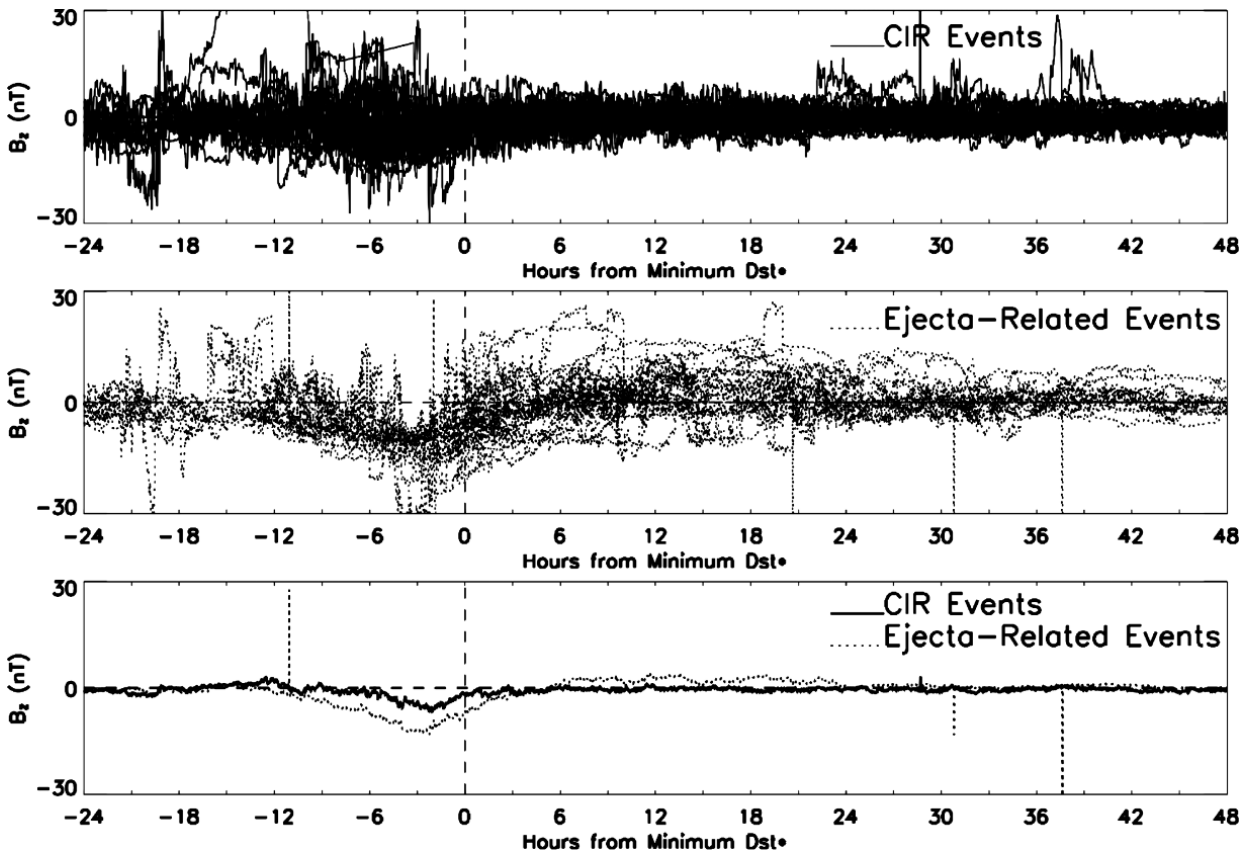


Figure 2. IMF B_z for all events in study. Panel A shows all CIR events, Panel B shows ejecta-related events, and Panel C shows a superposed epoch analysis for all events in the study. Vertical line shows time of minimum Dst^* .

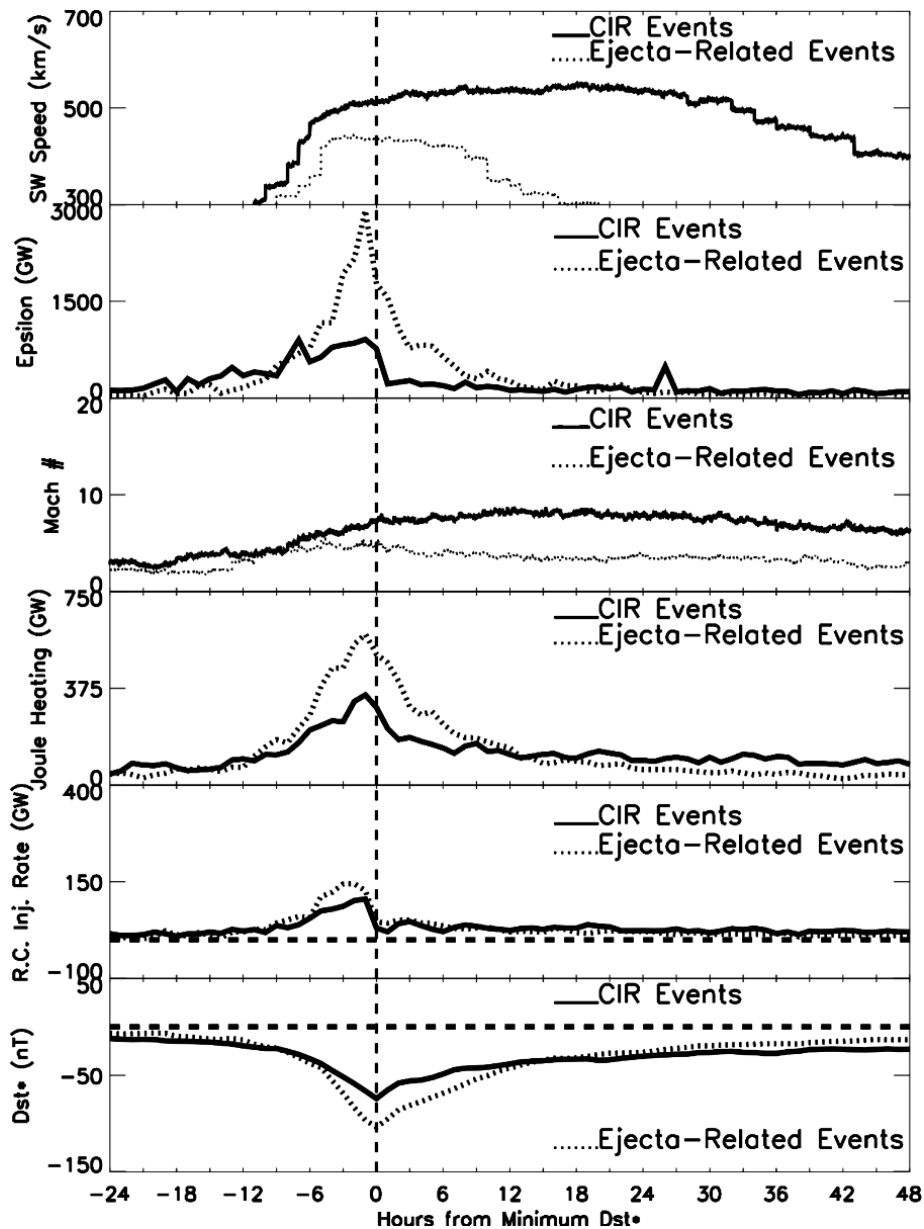


Figure 3. Superposed epoch analysis for solar wind input parameters (Solar wind speed, epsilon, and magnetosonic Mach number) and magnetospheric response (Joule heating, ring current injection rate, and Dst^*) for all events. Vertical line denotes time of minimum Dst^* .

margin as the input power. This difference in coupling efficiency will become more evident in later figures.

Figure 6 shows the input and output power for the main phase. While the input power for ejecta-driven storms is 70% larger than for CIR-driven storms, but the ring current injection rate is only 25% larger, the auroral precipitation rate is almost identical, and the Joule heating rate is 50% larger.

Figure 7 shows the input and output power for the recovery phase. The input power for recovery phase of the storms in the study averages 2.5 times larger for ejecta-driven than CIR-driven storms, and the ring current injection rate is nearly identical, the auroral precipitation rate is nearly identical, and the Joule heating is 33% larger. This gives further evidence of stronger coupling efficiency for CIR-driven storms.

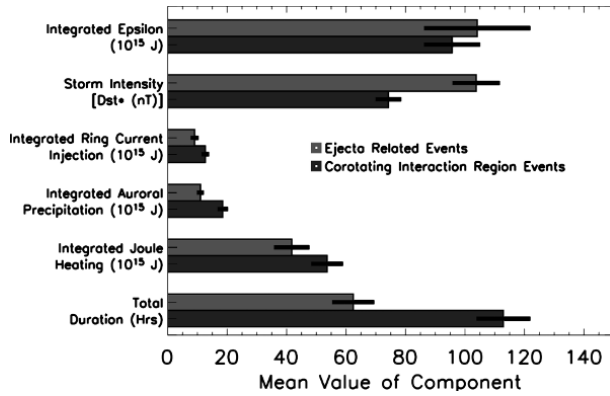


Figure 4. Bar graph depicting storm-integrated solar wind and magnetospheric response parameters for all events.

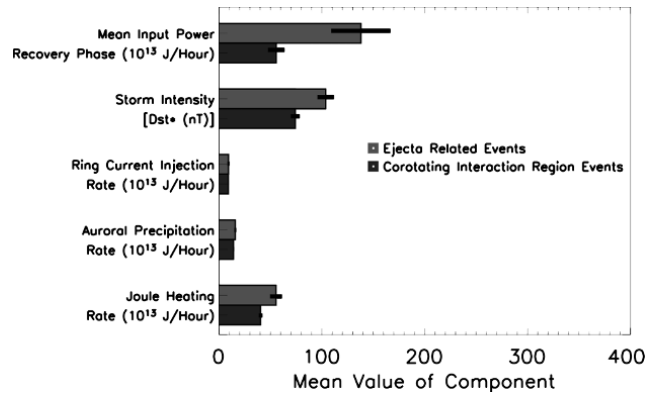


Figure 7. Bar graph depicting values of storm parameters averaged per hour over the storms' recovery phase for all events.

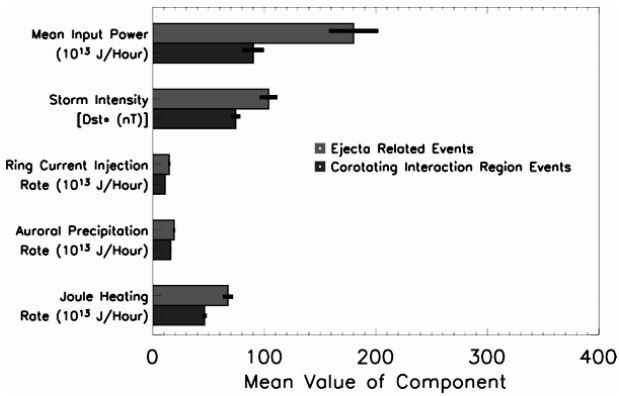


Figure 5. Bar graph depicting values of storm parameters averaged per hour over the storms' duration for all events.

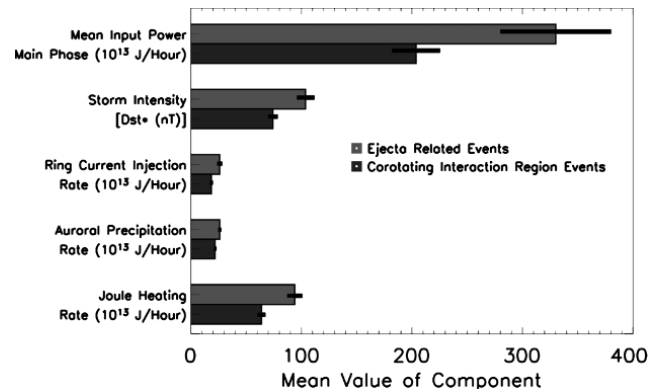


Figure 6. Bar graph depicting values of storm parameters averaged per hour over the storms' main phase for all events.

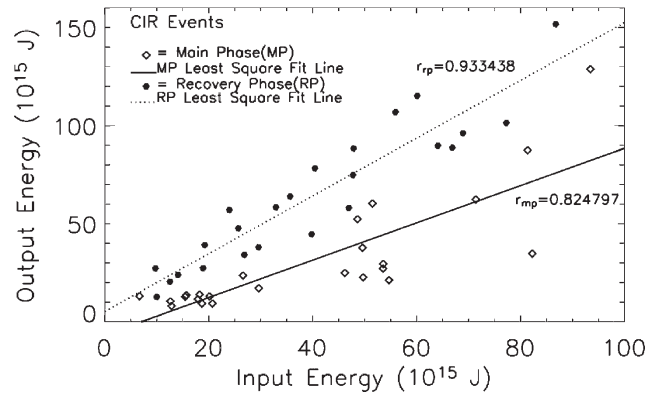
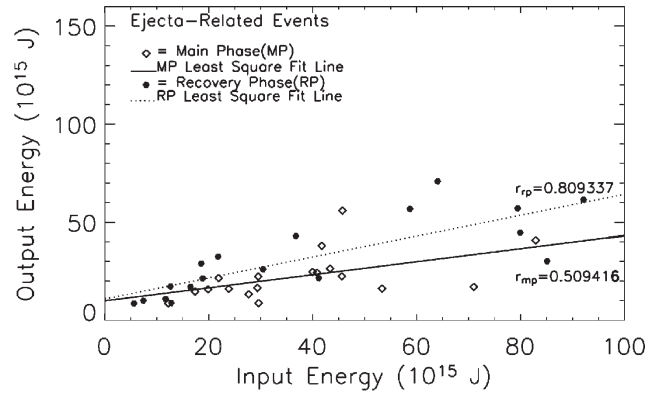


Figure 8. Panel A: Output energy versus input energy (integrated epsilon) for recovery phase and main phase for ejecta-driven storms, shown with linear fit and correlation coefficient for each. Panel B: Same parameters plotted for CIR-driven events.

Figure 8 illustrates in greater detail the differences observed in the preceding plots. In this figure is plotted the output energy on the y-axis and input energy on the x-axis. All storms in the dataset are plotted here. Panel A shows the data

for ejecta-driven events. Points corresponding to the main phase are indicated as diamonds, while points corresponding to recovery phase are indicated as filled circles. Two least squares fits are shown. The slopes of these lines approximate

Table 4. Table of energy input, output and geoeffectiveness

Main Phase	Input (10^{15} J)	Ring Current (10^{15} J)	Joule Heating (10^{15} J)	Auroral Precipitation (10^{15} J)	Output/Input
CIR-Driven	40	4.4	17	5.7	0.68
Ejecta-Driven	38	3.3	13	3.5	0.52
Recovery Phase	Input (10^{15} J)	Ring Current (10^{15} J)	Joule Heating (10^{15} J)	Auroral Precipitation (10^{15} J)	Output/Input
CIR-Driven	40	8.2	36	12	1.39
Ejecta-Driven	39	3.3	18	4.8	0.67

the coupling efficiency for main and recovery phases of storms. The slopes of these lines are very different, showing a much greater coupling efficiency for the CIR storms than for the ejecta storms, particularly in the recovery phase.

Table 4 shows the energy input and output for all events. The last column shows the output/input, which is a way to quantify the coupling efficiency. From this measure, the CIR-driven storms show a higher geoeffectiveness than do the ejecta-driven storms.

Figure 9 illustrates the recovery phase energies for storms in different stages of recovery. Panel A shows 20% recovery of the initial Dst^* excursion value, Panel B shows 40%, and Panel C shows 80%. The trend of CIR-driven storms containing greater output energies in the recovery phase is consistent throughout the panels.

5. DISCUSSION

5.1. Solar Wind Driving Conditions

From the B_Z plots in Figure 2 it is clear that the solar wind driving conditions are substantively different in CIRs than ejecta-related events. In the events studied the IMF B_Z moves, on average, towards a more northward configuration over time in CIRs, but keeps oscillating about $B_Z = 0$ for a long duration, typically days. These long-lasting variations could have the effect of driving the magnetosphere long after the main CIR-driven storm has begun to recover. Since it moves repeatedly back into southward B_Z configurations, sporadic reconnection may be driven and energy coupling may be correspondingly enhanced. The ejecta-related events typically show a clearer cutoff to the southward B_Z and the resulting storms appear to recover with less interruption.

During the CIR-driven storms' recovery phases, high-intensity long-duration continuous AE activity (HILDCAA) events are known to occur [e.g., *Tsurutani et al.*, 2004]. These events are a result of the continual driving of the storms during the recovery phase by high-speed solar wind streams and they are evident in the very slow recovery of Dst

for these events. It is believed that one mechanism of energy transfer during these events involves reconnection associated with the southward components of large amplitude interplanetary Alfvén waves that are present in high-speed streams [*Tsurutani et al.*, 2006 (this volume)].

Another aspect that may affect the coupling efficiency of CIRs is the high solar wind speed itself. As Figure 3 shows, the CIRs have, on average, markedly higher solar wind speeds. As has been pointed out by *Lu et al.* [1998], the kinetic energy flux is much greater than the Poynting flux for typical solar wind conditions. For example, *Lu et al.* [1998] found the kinetic power to be two orders of magnitude higher than the electromagnetic input (epsilon parameter) for the January 1997 storm. So if even a small percentage of kinetic energy flux is important in driving the magnetosphere, it could produce a large effect. Secondly, this also produces an increased magnetosonic Mach number, which may then increase the reconnection rate, thereby coupling more energy into the magnetosphere-ionosphere system. These important differences in the driving conditions may be responsible for enhanced efficiency of energy coupling from CIRs relative to ejecta.

5.2. Geoeffectiveness

Geoeffectiveness was extensively analyzed for the events in this study. It is clear from the bar graphs in Figure 4 that CIRs are more efficient at coupling energy into the magnetosphere than ejecta events. Even with the same input energy available to the system (epsilon), the output was measurably higher in every energy sink evaluated.

Since the CIR-driven events last typically so much longer than the ejecta events, the possibility that this longer duration was the cause of increased output was considered. Since ejecta storms typically produce large Dst^* excursions (see Figures), it could be the case that they couple more energy faster and the CIRs “catch up” only over the long duration of those storms. As seen in Figures 5, 6, 7, and 9, this was not found to be the case. If anything, the power output for CIR and ejecta events looked very similar, so the total energy

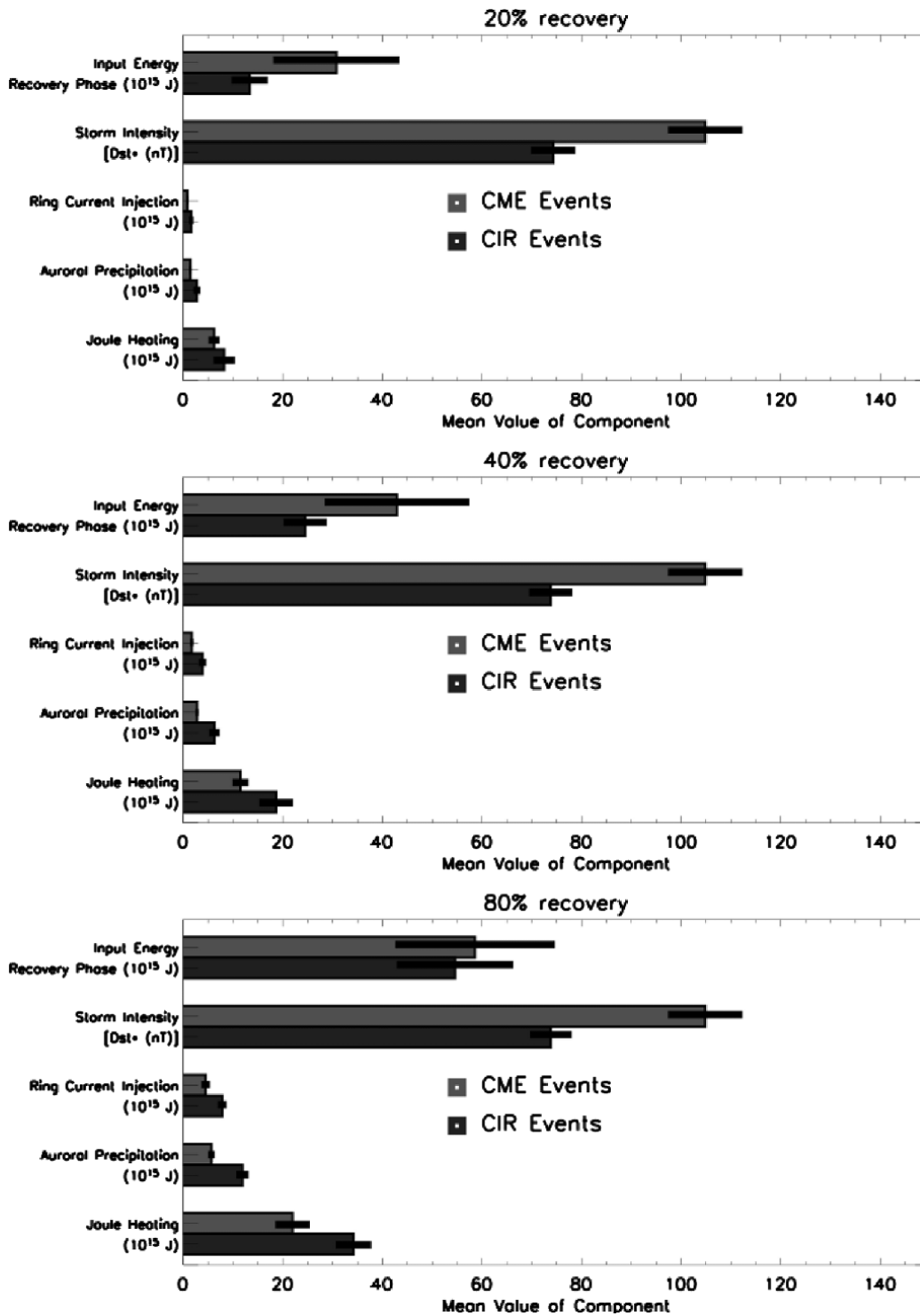


Figure 9. Bar graphs depicting storm parameters for different stages of recovery in all events in the study. Panel A: Values for storms after 20% of Dst^* recovery. Panel B: Values for storms after 40% of Dst^* recovery. Panel C: Values for 80% of Dst^* recovery.

output is higher for CIRs and the per-hour values are similar for both in the main phase. In Figure 9, further confirmation of this is seen as the trends remain for all stages of recovery.

Table 4 shows the output energy divided by the input energy, as an estimate of the coupling efficiency. Clearly, the CIRs are more geoeffective in these events than are the CMEs, and particularly so in the recovery phase.

The fact that the output/input for recovery phase in CIR-driven storms is greater than 1.0 indicates again the limitations of the epsilon parameter, as clearly the output cannot exceed the input. This indicates either that the Poynting flux was underestimated by epsilon or that there is a measurable influence from another type of energy coupling, for example the kinetic energy flux.

5.3. Recovery Phase Energy Coupling

It is in the recovery phase where the dynamics of CIR and ejecta storms diverge the most. Figure 7 shows the power output from both types of storms in recovery phase, where full recovery is considered to be when the Dst^* recovers to 80% of its initial value. Even though the estimated input power for ejecta-driven storms is about 2.5 times that for CIRs, the output power is very similar. This greater coupling efficiency appears as a consistent pattern, as shown clearly in Figures 8 and 9 and Table 4.

From Figure 8 it is clear that the recovery phase behavior of CIR and ejecta-driven storms is very different. Both the clear correlation between input and output energy in the recovery phase and the high geoeffectiveness suggest that the phase of the storm that exists after the Dst^* minimum in a CIR-driven event may not be a pure recovery. This may be due to the repeated excursions into southward B_Z that are characteristic of the solar wind conditions in CIR events. Ejecta-driven events showed weaker responses to recovery-phase driving, which likely accounts for their faster recovery and overall shorter duration.

6. CONCLUSIONS

From this study, it has been shown that the solar wind-magnetosphere energy coupling of CIR-driven and ejecta-driven storms differ in several important properties. In particular, while the ejecta-driven events typically produce greater Dst excursions than the CIR events, the CIRs are more geoeffective in the sense of greater overall energy output than are the ejecta events. When CIR and ejecta events with the same input energies are compared, CIR events have greater energy output. Output power is similar for the two types of events in the storms' main phases, but in recovery phase the CIRs have less input power and the similar output power to ejecta events. More specifically, the measured

geoeffectiveness during the recovery phases of CIR-driven storms is double that of ejecta-driven events. These key differences, especially in the recovery phase, are likely due to the rapidly oscillating IMF B_Z that is typical of CIR-driven events well into storm recovery and the energy coupling that produces.

Acknowledgments. The authors acknowledge Ian Richardson for identification of CIR and ejecta events. Work of NT and EM is supported by NSF Career Grant ATM-0454685. EM was also supported by the NIH MARC program. The CEDAR database is sponsored by the NSF. Intersatellite calibration work by BE is supported by National Space Weather Program Grant # 0208145. NT acknowledges fruitful discussions and inspiration from the Chapman Conference on Corotating Solar Wind Streams and Recurrent Geomagnetic Activity. The authors also acknowledge OMNIWeb and the Kyoto Geophysical Data Center for making solar wind and Dst data available and convenient, and gratefully thank the WIND instrument teams for making their data available for use. Finally, the authors thank the reviewers for their valuable comments.

REFERENCES

- Baker, D.N., N.E. Turner, and T.I. Pulkkinen, Energy transport and dissipation in the magnetosphere during geomagnetic storms, *J. Atmos. Solar-Terr. Phys.*, 63, 421-429, 2001.
- Bargatze, L.F., R.L. McPherron, and D.N. Baker, Solar wind-magnetosphere energy input functions, in *Solar Wind-Magnetosphere Coupling*, Edited by Y. Kamide and J.A. Slavin, 101-109, 1985.
- Campbell, W.H., Geomagnetic storms, the Dst ring current myth and log-normal distributions, *J. Atmos. Solar-Terr. Phys.*, 58, 1171-1187, 1996.
- Chun, F.K., D.J. Knipp, M.G. McHarg, G. Lu, B.A. Emery, S. Vennerstrom, O.A. Troshichev, Polar cap index as a proxy for hemispheric Joule heating, *Geophys. Res. Lett.*, 26, 1101-1104, 1999.
- Dessler, A.J., and E.N. Parker, Hydromagnetic theory of magnetic storms, *J. Geophys. Res.*, 64, 2239-2259, 1959.
- Echer, E. and W.D. Gonzalez, Geoeffectiveness of interplanetary shocks, magnetic clouds, sector boundary crossings and their combined occurrence, *Geophys. Res. Lett.*, 31, doi:10.1029/2003GL019199, 2004.
- Emery, B.A., D.S. Evans, M.S. Greer, K. Kadinsky-Cade, E. Holeman, F.J. Rich and W. Xu, NOAA and DMSP Intersatellite Adjusted Hemispheric Power Data Sets, <http://cedarweb.hao.ucar.edu> and <http://cedarweb.hao.ucar.edu/instruments/ehp.html>, *Coupling, Energetics and Dynamics of Atmospheric Regions (CEDAR) Database* at the National Center for Atmospheric Research (NCAR), Boulder, Colorado, USA, 2005.
- Emery, B.A., D.S. Evans, M.S. Greer, K. Kadinsky-Cade, E. Holeman, F.J. Rich and W. Xu, The low energy auroral electron and ion hemispheric power after NOAA and DMSP intersatellite adjustments, *NCAR Scientific and Technical Report, TN-470 + STR*, 2006.
- Feldstein, Y.I., A.E. Levin, J.U. Kozyra, B.T. Tsurutani, A. Prigancova, L. Alperovich, W.D. Gonzalez, U. Mall, I.I. Alexeev, L.I. Gromova, and L.A. Dremukhina, Self-consistent modeling of large-scale distortions in the geomagnetic field during the 24-27 September 1998 major magnetic storm, *J. Geophys. Res.*, 110, A11214, doi:10.1029/2004JA010584, 2005.
- Gonzalez, W.D., B.T. Tsurutani, A.L.C. Gonzalez, E.J. Smith, F. Tang, and S.-I. Akasofu, Solar wind-magnetosphere coupling during intense magnetic storms (1978-1979), *J. Geophys. Res.*, 94, 8835-8851, 1989.
- Gonzalez, W.D., B.T. Tsurutani, and A.L. Clúa de Gonzalez, Interplanetary origin of geomagnetic storms, *Space Science Reviews*, 88: 529-562, 1999.

- Huttunen, K.E., H.E. Koskinen, R. Schwenn, Variability of magnetospheric storms driven by different solar wind perturbations, *J. Geophys. Res.*, 107, doi:10.1029/2001JA900171, 2002.
- Knipp, D.J., B.A. Emery, M. Engebretson, X. Li, A.H. McAllister, T. Mukai, S. Kokubun, G.D. Reeves, D. Evans, T. Obara, X. Pi, T. Rosenberg, A. Weatherwax, M.G. McHarg, F. Chun, K. Mosely, M. Codrescu, L. Lanzerotti, F.J. Rich, J. Shriver, and P. Wilkinson, An overview of the early November 1993 geomagnetic storm, *J. Geophys. Res.*, 103, 26197, 1998.
- Knipp, D.J., W.K. Tobiska, and B.A. Emery, Direct and indirect thermospheric heating sources for solar cycles 21-23, *Solar Physics*, 224, 495-505, 2004.
- Lu, G., D.N. Baker, R.L. McPherron, C.J. Farrugia, D. Lummerzheim, J.M. Ruohoniemi, F.J. Rich, D.S. Evans, R.P. Lepping, M. Brittnacher, X. Li, R. Greenwald, G. Sofko, J. Villain, M. Lester, J. Thayer, T. Moretto, D. Milling, O. Troshichev, A. Zaitzev, V. Odintzov, G. Makarov, and K. Hayashi, Global energy deposition during the January 1997 magnetic cloud event, *J. Geophys. Res.*, 103, 11,685-11,694, 1998.
- Monreal-MacMahon, R. and W.D. Gonzalez, Energetics during the main phase of geomagnetic superstorms, *J. Geophys. Res.*, 102, 14,199-14,207, 1997.
- O'Brien, T.P., and R.L. McPherron, An empirical phase space analysis of ring current dynamics: Solar wind control of injection and decay, *J. Geophys. Res.*, 105, 7707-7719, 2000.
- O'Brien, T.P., R.L. McPherron, and M.W. Liemohn, Continued convection and the initial recovery of *Dst*, *Geophys. Res. Lett.*, 29(23) 2143, doi:10.1029/2002GL015556, 2002.
- Ohtani, S., M. Nosé, G. Rostoker, A.T.Y. Lui, and M. Nakamura, Storm-substorm relationship: Contribution of the tail current to *Dst*, *J. Geophys. Res.*, 106, 21999-21209, 2001.
- Perreault, P., and S.-I. Akasofu, A study of geomagnetic storms, *Geophys. J. R. Astr. Soc.*, 54, 547, 1978.
- Pulkkinen, T.I., N. Ganushkina, D.N. Baker, N.E. Turner, J.F. Fennell, J. Roeder, T.A. Fritz, M. Grande, B. Kellett, G. Kettmann, Ring current ion composition during solar minimum and rising solar activity: Polar CAMMICE/MICS results, *J. Geophys. Res.*, 106, 19131-19147, 2001.
- Sckopke, N., A general relation between the energy of trapped particles and the disturbance field near the Earth, *J. Geophys. Res.*, 71, 3125-3130, 1966.
- Tsurutani, B.T., W.D. Gonzalez, F. Guarneri, Y. Kamide, X. Zhou, and J.K. Arballo, Are high-intensity long-duration continuous AE activity (HILD-CAA) events substorm expansion events?, *J. Atmos. & Solar-Terr. Phys.*, 66, 167-176, 2004.
- Tsurutani, B.T., N. Gopalswamy, R.L. McPherron, W.D. Gonzalez, G. Lu, F.L. Guarneri, Magnetic storms caused by corotating solar wind streams, *AGU Geophysical Monograph Series, this volume*, 2006.
- Turner, N.E., D.N. Baker, T.I. Pulkkinen, and R.L. McPherron, Evaluation of the tail current contribution to *Dst*, *J. Geophys. Res.*, 105, 5431-5439, 2000a.
- Turner, N.E., Solar wind-magnetosphere coupling and global energy budgets in the Earth's magnetosphere, *Doctoral Dissertation*, 2000b.
- Turner, N.E., D.N. Baker, T.I. Pulkkinen, J.L. Roeder, J.F. Fennell, and V.K. Jordanova, Energy content in the storm time ring current, *J. Geophys. Res.*, 106, 19149-19156, 2001.
- Vichare, G., S. Alex, and G.S. Lakhina, Some characteristics of intense geomagnetic storms and their energy budget, *J. Geophys. Res.*, 110, A03204, doi:10.1029/2004JA010418, 2005.
- Weiss, L.A., P.H. Reiff, J.J. Moses, R.A. Heelis, and B.D. Moore, Energy dissipation in substorms, in *Substorms 1*, edited by B. Hultqvist and S. Akasofu, 309-318, 1992.
- Zhang, J., M.W. Liemohn, J.U. Kozyra, B.J. Lynch, and T.H. Zurbuchen, A statistical study of the geoeffectiveness of magnetic clouds during high solar activity years, *J. Geophys. Res.*, 109, A09101, doi:10.1029/2004JA010410, 2004.

Niescja E. Turner and Elizabeth J. Mitchell, Physics and Space Sciences, Florida Institute of Technology, Melbourne, Florida 32901

Delores J. Knipp, Physics Department, US Air Force Academy, USAFA, Colorado 80840

Barbara A. Emery, High Altitude Observatory, National Center for Atmospheric Research, Boulder, Colorado 80307